J Mater Sci: Mater Electron (2024) 35:162

Improvement in optoelectronics and photovoltaic properties of p-Co_3O_4/n-ZnO hetero-junction: effect of deposition time of sprayed Co_3O_4 thin films

Warda Darenfad[1,*], Noubeil Guermat[2], Nadir Bouarissa[3,*], Fatima Zohra Satour[4], Ameur Zegadi[4], and Kamel Mirouh[1]

[1] *Thin Films and Interfaces Laboratory (LCMI), University of Constantine 1, 25000 Constantine, Algeria*
[2] *Department of Electronics, Faculty of Technology, University of M'sila, P.O.Box 166, Ichebilia, 28000 M'sila, Algeria*
[3] *Laboratory of Materials Physics and Its Applications, University of M'sila, 28000 M'sila, Algeria*
[4] *LCCNS, Faculté de Technologie, Université Ferhat Abbas - Sétif 1, 19000 Setif, Algeria*

Received: 9 October 2023
Accepted: 26 December 2023

ABSTRACT

Spinel thin films Co_3O_4 have been deposited at a temperature of approximately 400 °C using spray pyrolysis. The testimony process was carried out with different deposition times (4, 5, 6, and 8 min), indicating that the films were grown for varying durations. The objective of varying deposition times of the thin films of Co_3O_4 was to optimize the fabrication of a hetero-junction between Co_3O_4 and ZnO. XRD, SEM and Raman investigations showed that pure cubic Co_3O_4 with an irregular spindle shaped particles have been successfully obtained. The films' thickness increased under prolonged preparation times leading to a denser surface. The optical measurements revealed that the thin layer with a deposition time of 8 min attained a total absorbance of 98% in the apparent spectrum with a band gap of 1.27 eV. The I–V characteristics recorded of FTO/ZnO/Co_3O_4/Au cells showed that all devices exhibiting a rectifying behavior with a perfect factor that varies between 3.87 and 1.64. Our results suggest that Co_3O_4 at 8 min with a carrier density of 2.414×10^{14} cm^{-3} and high absorbance is potentially a competitive hole transport material in spinel solar cells, and, the recorded characteristics of the photovoltaic phenomenon were noted a short circuit current of 1.302 mA, an open circuit voltage of 369 mV and a fill factor of 32%.

1 Introduction

These last few years, Si [1], Cu_2ZnSnS_4 [2], $CuInSe_2$ [3], CdTe [4], GaAs [5], InAs [6], and CdO [7] are the key inorganic semiconductors thoughtfully investigated for photovoltaic applications. Yet, certain boundaries limit further developments of such materials: the indirect gap of Si, their rarity, toxicity and high cost. Hence, besides improving the efficiency of solar cells, it is indispensable to search for novel compounds with appropriate semiconductor properties so as to broaden horizons. As a result, metallic oxides founded on solar

Address correspondence to E-mail: daranfed.warda@umc.edu.dz; N_bouarissa@yahoo.fr

https://doi.org/10.1007/s10854-023-11909-2
Published online: 17 January 2024

cells have an unlimited potential to overcome most of the troubles encountered in conventional solar cells. The "all oxide" photovoltaic approach is very interesting since it offers better chemical stability, has a negligible toxicity and for the plenty for a lot of metal oxides enabling, thus, solar cells manufacturing under normal status. Metal oxides are commonly utilized as components in electronics as transparent conductive electrodes. The little metal oxides that are utilized as solar absorbers, mostly p-type Cu_2O based with a gap of 1.9–2.2 eV [8], are inappropriate to encompass the solar spectrum, resulting in solar conversion efficiencies that did not exceed 3.22% [9]. Actually, there is a need for new absorbing materials to be able to achieve higher solar cells' performances based on low-cost technology and environmentally caring. A solution might be found in transition metal oxides that crystallize in a spinel-like structure. Among the spinel oxides, cobalt oxide is one of the further important materials owing to its remarkable feathers and thermal stability. It has three celebrated valence states, cobalt oxide (COO), cobaltic oxide (Co_2O_3) and cobaltite (Co_3O_4) [10]. The further steady phase of the cobalt oxide framework is a composite with joint parity [Co^{+2} $Co^{+3}]_2O^{-2}$ [10]. Recently, Co_3O_4 is attracting increasing interests in numerous applied fields: solar selected absorbers [11], anodic electro-chromic materials in clever counter junk, negative electrodes in lithium-ion batteries [12], sensing, protective coatings or pigment for glasses, ceramics, etc… Cobalt oxide Co_3O_4 has a spinel phase and is a p-type material with a great chemical stability at high temperatures, an excellent mechanical strength and was reported to have different direct gap values ($Eg_1 = 1.5$ eV, $Eg_2 = 2.1$ eV) [10]. Various techniques are utilized to grow Co_3O_4 thin films that is: sputtering, chemical bath deposition [13], sol-gel [14] and spray pyrolysis [15]. The latter is simple, uses traditional means, and requires low manufacturing costs. It is excellent for depositing homogeneous and adherent semiconductor films. Its performance is locally possible, having the benefit of large-scale productions. Scientists typically fine-tune the parameters of spray pyrolysis to attain a consistent and uniform deposition. For example, Balakarthikeyan et al. [16] have demonstrated the effect of annealing temperature from 275 to 375 °C on the various optoelectronic properties of the Co_3O_4 thin films using low-cost nebulizer spray pyrolysis for photo-sensing applications. The Co_3O_4 (350 °C) produce high photocurrent (8.84×10^{-7}A), external quantum efficiency (11.6%), detectivity (3.5×10^9 Jones), responsivity (4.99×10^{-2} AW^{-1}) and has the shortest rise/decay time among the constructed photo-detectors. Daranfed et al. [10], have developed Co_3O_4 films at different precursor concentrations (0.05 to 0.15 mol/l) at a constant substrate temperature of 400 °C and a deposition time of 4 min, using the spray pyrolysis technique for photovoltaic application. The various characteristics demonstrate that the layer prepared with a concentration of 0.15 mol/l exhibits robust p-type electrical semiconductor properties as well as excellent sunlight absorbance. Manickam et al. [17], have undertook the deposition of thin films of cobalt oxide exhibiting a single-phase cubic structure on preheated glass substrates, using the spray pyrolysis nebulizer technique with variations in solution pH. An in-depth analysis of the structural, optical, morphological and electrical properties of these layers was carried out. Crystals with a cubic structure were identified using X-ray diffraction patterns, showing a preferential orientation along the (220) direction. The transmittance of Co_3O_4 increases proportionally to the increase in pH of the solution. The band gap values of the Co_3O_4 layers are in the range of 2.105–2.347 eV for high-energy regions and 1.74–1.806 eV for low-energy regions. Scanning electron microscopy images reveal different morphologies, such as spherical particles, hexagonal-shaped particles, and grain coalescence depending on the solution pH. The maximum electrical conductivity at room temperature (1.94×10^{-4} S/cm) is reached for a pH of 6.

The present working is devoted the survey of the impact of the prepared Co_3O_4 thin films' thicknesses on their structural, morphological, optical, and electrical proprieties. Thereafter, the fabrication and the characterization results of p-Co_3O_4/n-ZnO heterojunctions are presented.

2 Experimental procedures

Co_3O_4 thin films are get ready on glass substrates utilizing the spray pyrolysis procedure. The starting resolution contained 0.05 mol/l of cobalt nitrate ($Co(NO_3)_2.6H_2O$) diluted in distilled water. The latter was preferred for its abundance and low cost. Little lowering of hydrochloric acid were appended to the settlement to ensure the complete dissolution of ($Co(NO_3)_{2*}6H_2O$). The mixing was stirred at room temperature for 30 min prior to deposition with

solution pH 6 and the viscosity value equal to 1.133 mPa.s. Different deposition duration times (4, 5, 6, and 8 min) were undertaken. A distance of 22 cm was kept between the atomizer and the substrates. The transporter gas (compressed air) and the settlement were fed into a pulverization nozzle at a pre-adjusted constant atomization pressure (2 bar) and the substrate temperature was maintained at 400 °C. The experimental apparatus employed for the fabrication of our films is of the Holmarc type, as depicted in Fig. 1.

The measurement of the thickness of our films is done using a DECTAK3 type profilometer. The structural domains were established by XRD utilizing a Philips X' Pert framework (a CuKα striking off source, a wavelength of 1.541874 Å), and Raman spectroscopy. The films morphology and composition were examined utilizing a scanning electron microscope (SEM) coupled with an energy dispersive system (EDX). The optical transmission was performed in UV–visible spectrum (i.e., 300 to 1000 nm) utilizing Shimadzu UV–3101 PC spectrophotometer. The Hall Effect technique was utilized to assess the electrical properties of the films at RT. The hetero-junction was fabricated with the following layer sequence: Glass/FTO/ZnO/Co_3O_4/Au (Fig. 2). The Co_3O_4 thin film was prepared using spray pyrolysis, with a testimonial time of 8 min. ZnO thin film get also ready using spray pyrolysis. The solution used for deposition contained 0.1 mol/l of zinc acetate dihydrate ($Zn(CH_3COO)_2.2H_2O$) dissolved in methanol. The substrate temperature is preserved at 350 °C, and the testimony time is 10 min. The current–voltage (I–V) representative of the hetero-structure was written down utilizing a Sony Tektronix 370 curve tracer.

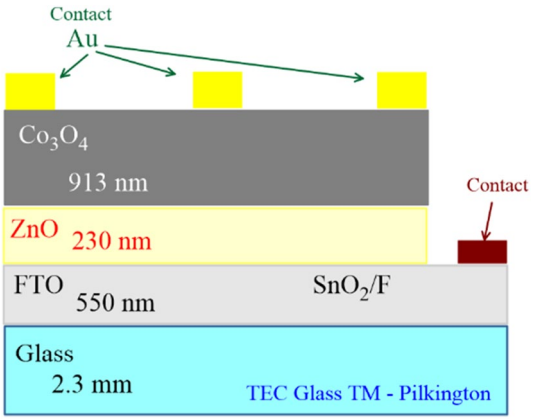

Fig. 2 Diagram of the device Glass/FTO/ZnO/Co_3O_4/Au

3 Results and discussion

3.1 Microstructure and morphology

Figure 3 exhibits the X-ray diffraction patterns of Co_3O_4 thin films get ready with diverse testimony duration times. Peaks specifically related to Co_3O_4, namely (111), (220), (311), (400), (422), (511), and (440) and located at $2\theta = 18.90°$, 31.30°, 36.81°, 44.90°, 55.70°, 59.50°, and 64.92º, respectively, are noticeable in this Figure. These diffraction peaks indicate that the films are polycrystalline with a cubic spinel structure

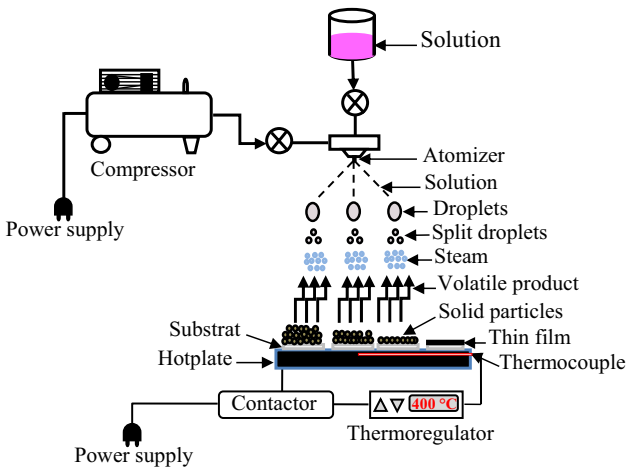

Fig. 1 Schematic diagram of spray pyrolysis the Holmarc type

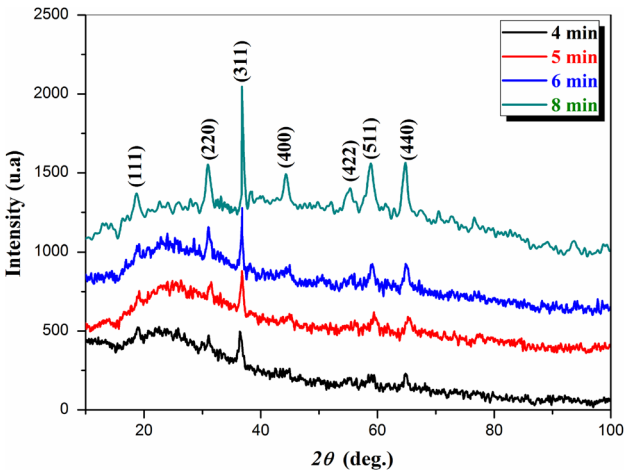

Fig. 3 XRD patterns of Co_3O_4 thin films deposited at different deposition times

(JCPDS card no 42-1467) in accordance with several reported studies [10, 15]. The films came out with a preferred orientation of (311). The intensity of the diffraction peaks is seen to augment with prolonged testimony times. As a result, it can be concluded that longer deposition duration times improve the material crystallinity due better thermal decompositions of the precursor. This result agrees well with that of Patel et al. [18] on elaborated Co_3O_4 thin films using the sputtering technique. Herein, the Co_3O_4 phase is more stable since no other peaks corresponding to cobalt oxides like CoO or Co_2O_3 were picked up in accordance with the reported results of Louardi et al. [15] and Manogowri et al. [19] who had used the spray technique.

The films crystallite stature (D) was estimated from the most intense peak namely (311) using Debye Scherrer formula [20–22]. Figure 4 depicts the change of D versus the testimony duration time. It is clear that D, increases with augmenting the deposition period time. Such an increase in D reflects the improvement in the crystallinity of the films, and is in nice accord with XRD patterns. In fact, prolonged deposition period times led to a higher Co concentration and a faster nucleation in the films' growth, and thus yielding a larger Prasada Rao et al. [23] have argued that this behavior could be attributed to the quantity of solute (cobalt nitrate) scoping the substrate surface to make agglomerations or greater crystallites' sizes. The strain (ε) values were obtained utilizing the subsequent expression [24, 25]:

$$\varepsilon = \frac{\beta \cos\theta}{4} \tag{1}$$

The dislocation density (δ) is estimated by the following relation [20]:

$$\delta = \frac{1}{D^2} \tag{2}$$

Furthermore, Fig. 4 illustrates that the strain and dislocation density exhibit a decrease proportional to the increase in deposition time, and vary inversely proportional to the crystallite size. This reduction observed in the density of dislocations and deformation suggests a reduction in imperfections within the crystal lattice, particularly at the grain boundaries. The reduction in micro-strain and dislocation density values suggests the alleviation of stress and the healing of defects, corresponding to an increase in solute concentration [26].

The structure of Co_3O_4 films was examined versus the deposition time using Raman spectroscopy. The recorded spectra at a laser wavelength of 633 nm are illustrated in Fig. 5. Five modes are present; the peaks obtained are characteristic of vibration modes of the Co–O bond. The wavenumbers at which these Raman peaks are detected are around 190, 467, 512, 602, and 670 cm^{-1} corresponding to the three symmetries phonon F_{2g}, Eg and A_{g1} in agreement with those signaled in references [27, 28]. The A_{g1} mode is attributed to a vibration that is greatly specified by octahedral cations where Co^{+3} occupies octahedral

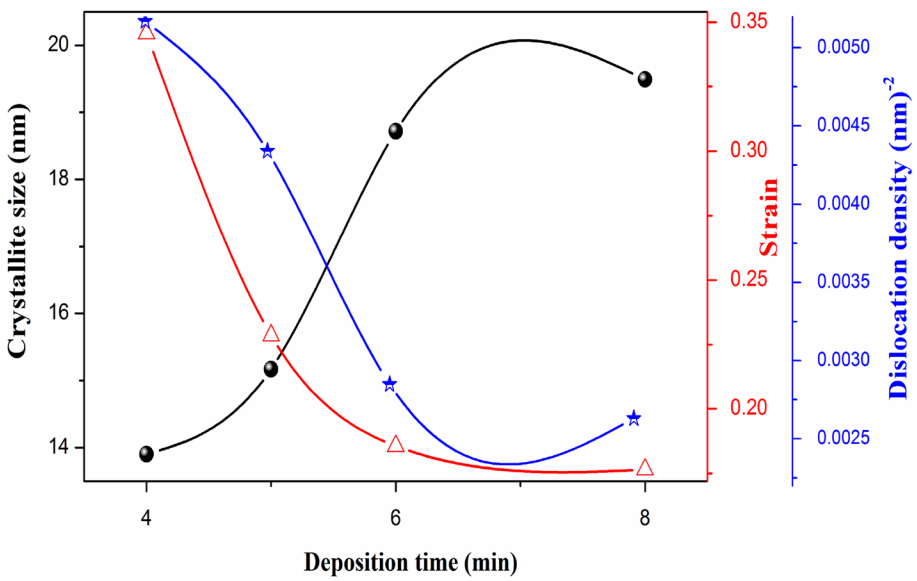

Fig. 4 Crystallite size, strain, and dislocation density versus the deposition periodic time

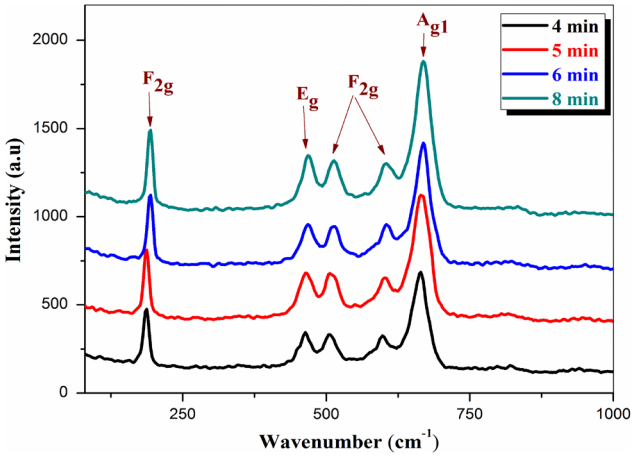

Fig. 5 Micro-Raman spectra of Co_3O_4 thin films deposited with diverse deposition times

locations [29]. $F_{2g(2)}$, $F_{2g(3)}$ and Eg modes accounted for the combined vibrations of tetrahedral and octahedral locations [30, 31]. Meanwhile, $F_{2g(1)}$ is attributed to tetrahedral locations [32]. The Raman spectra results confirm the attendance of Co_3O_4 stage with a cubic spinel structure as deducted from XRD reports. As shown in Fig. 4, we may observe that the intensity of peaks augments by augmenting the films' thickness. Such a behavior is acceptable since the number of bonds engaged in the vibration mode increases with the material quantity making up the films (densification of the films).

Figure 6 depicts typical EDS spectra obtained from part of Co_3O_4 thin films as deposited during the various undertaken duration times (4, 5, and 8 min). They confirm the attendance of Co and O making up the films. Another chemical factors (Si and Ca) from the substrates are also detected. We can plainly note that the films' atomic composition is inducted by the films' thickness (i.e., the testimony duration). As a result, the film deposited with brief times (4 and 5 min) led to the formation of O-rich cobalt oxide. This is attributed to the chemisorbed oxygen from atmospheric air. Herein, tangible quantities of Si and Ca of the substrate are detected owing to the thin thickness of the film. Meanwhile, the films, which were deposited during 8 min, were Co-rich cobalt oxide. The atomic percentage of cobalt content in the films is seen to increase with prolonged deposition times. Indeed, as the film gets thicker, the intensity of EDS peaks of Si and Ca are seen to decrease. The film whose deposition lasted 8 min has a composition

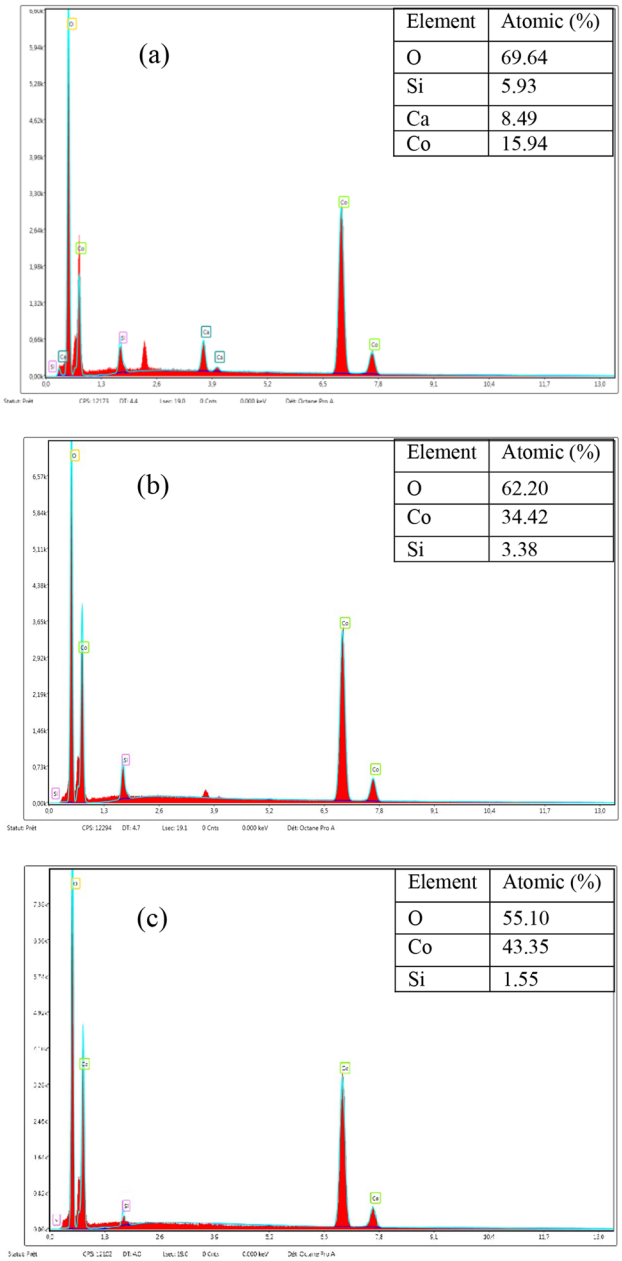

Fig. 6 EDS spectra of deposited Co_3O_4 films with various deposition periods **a** 4 min, **b** 5 min and **c** 8 min

close to stoichiometry, yielding a ratio of O:Co equal to 1.33, a value close to ideal [10].

The films surfaces' morphology is examinedi by scanning electron microscopy (SEM). Figure 7 depicts SEM micrographs of Co_3O_4 thin films as prepared with various deposition times. For shorter deposition times (i.e., 4 and 5 min corresponding to Fig. 7a and b, respectively), the surface morphology consists of wire alike structures that are linked cross and

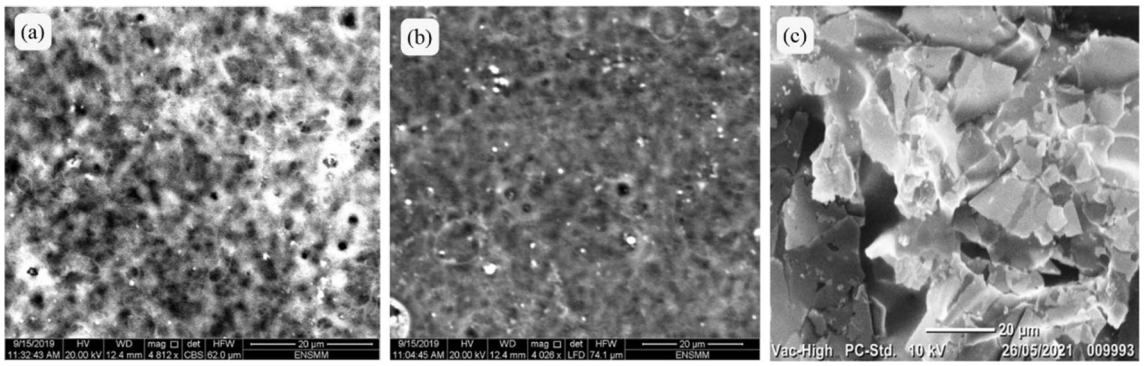

Fig. 7 SEM micrographs of Co_3O_4 thin films deposited with various deposition periods: **a** 4 min, **b** 5 min and **c** 8 min

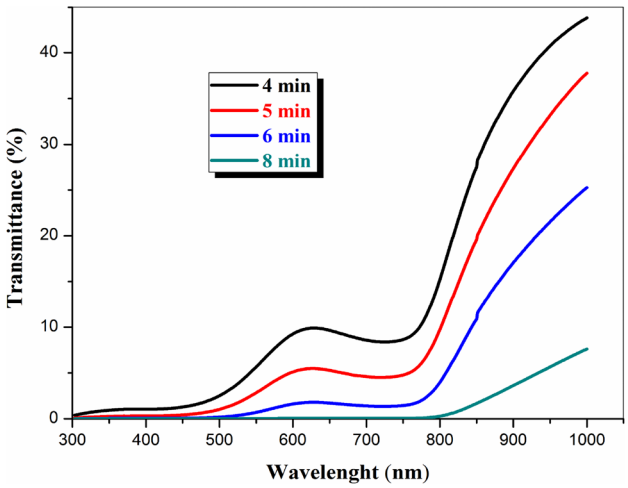

Fig. 8 UV–visible transmittance spectral distributions of the prepared Co_3O_4 thin films

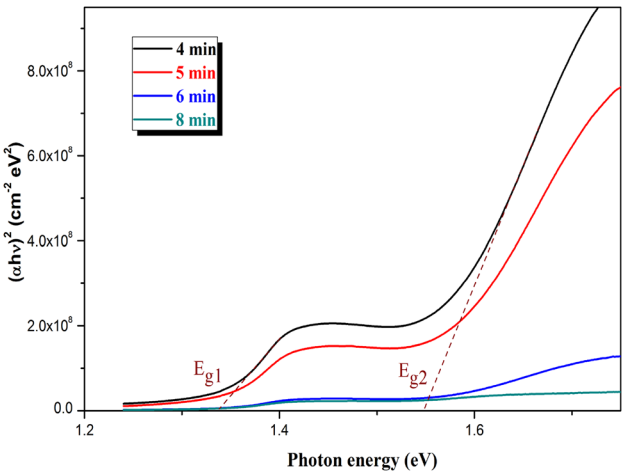

Fig. 9 Tauc's plots of Co_3O_4 thin films used for optical bandgap determination

interconnected. The porosity nature of the 4 min film was high. The SEM micrograph of the sample that took 8 min to elaborate, shown in Fig. 7c, consists of a dense surface and contains irregular spindle grains, which are randomly distributed over the film surface. Owing to its properties, this sample was chosen as a basis for a solar cell application.

3.2 Optical properties

The transmittance spectral distributions of the Co_3O_4 films with different deposition times (from 4 to 8 min) using UV-visible spectrophotometer are illustrated in Fig. 8. For the samples whose time to grow took between 4 and 6 min, these have shown high values of the transmittance in the near infrared region (IR) and lower ones in the visible part of the spectrum. This behavior may be due to the films' opaqueness. Two absorption edges in the spectra of transmittance are noticeable around 570 and 810 nm. As for the Co_3O_4 thin film whose deposition time took 8 min, only a single edge is detected in the near IR ($\lambda \approx 800$ nm). The film showed a very weak light transmission rate (around 7%), characteristic of the good absorbent film. These results confirm the existence of two direct bandgaps in accordance with existing reported studies [33]. In addition, it is worth noting the decrease in the films' transparency from 45 to 7% when augmenting the time in elaborating the films. Such a behavior may be due to the film's thickness.

The bandgap is specific from the plot of $(\alpha h\nu)^2$ versus the photon energy ($h\nu$) and is shown in Fig. 9. Two linear areas are distinct, pointing out the existence of two separate energy accounts of the gap, that can be attributed to the spin-orbit splitting of the valence band of Co_3O_4. The worth of Eg, that are acquired

by extrapolating the right linear portion to Y-axis = $(\alpha h\nu)^2 = 0$, are introduced in Table 1. The lower values of the gap vary between 1.41 and 1.45 eV, are usually combined with the charge transference ($O^{-2} \rightarrow Co^{+3}$), whereas the higher worth, whose variations lay down between 1.47 and 2.02 eV, are coupled to the charge transference ($O^{-2} \rightarrow Co^{+2}$). These founding's are in right accordance with the reported datum [34, 35] and which suggests the possibility of valence band degeneracy.

According to Table 1, it is notable that E_{g1} exhibits a decreasing trend with the increase in deposition time, indicating a concurrent increase in the film thickness. This trend is coupled with a decline in the values of E_{g1}, ranging from 1.34 to 1.27 eV. The change in the optical gap can be elucidated by the growth in crystallite size within thin films, which is associated with the quantum size effect. This phenomenon implies that the crystallite size grows proportionally with the thickness of the film. Additionally, the reduction in the band-gap energy may be correlated with a tendency towards decreasing deformation and dislocation density (as shown in Fig. 4), influencing the inter-atomic spacing of the semiconductors and, consequently, impacting the gap energy. In summary, the observed variations in the optical properties of the films appear intricately linked to parameters such as thickness, crystallite size, and crystal enhancement [35, 36]. This enhancement is a consequence of the stoichiometry of the film network, suggesting that defects and impurities originating from interstitial O atoms diminish as the deposition time increases. Consequently, we observe a reduction in the optical gap and Urbach energy with the prolonged deposition time (Table 1). Ravi Dhas et al. [26] prepared Co_3O_4 films with different solution molarities (0.05–0.20 M) through nebulizer spray technique.The value E_{g1} indicates the true band gap of Co_3O_4.The variation of E_{g1} (2.1 eV–1.75 eV) manifests a red shift, which may be correlated to the crystalline defects such as dislocation, stress, and stacking faults reduced with increase in solution concentration. It is evident that the sample fabricated for 8 min exhibits reduced gap energy, which results in significant absorption at lower wavelengths. These characteristics make these films promising candidates as absorbent layers in solar cell manufacturing.

Table 1 Optical energy-gaps and Urbach's energy of prepared Co_3O_4 thin films

Sample	E_{g1} (eV)	E_{g2} (eV)	E_{u1} (eV)	E_{u2} (eV)
4 min	1.34	1.51	0.8	0.69
5 min	1.33	1.53	0.78	0.67
6 min	1.29	1.5	0.76	0.65
8 min	1.27	–	0.75	–

3.3 Electrical properties

The electrical properties of Co_3O_4 thin films are characterized at room temperature using the Hall Effect technique. The carrier concentration, Hall mobility and electrical resistivity are presented in Table 2. According to Hall constant sign, all prepared thin films were p-type conductive [37, 38]. The increase in the resistivity is presumably owing to the decrease in clear carriers' concentration. The resistivity of Co_3O_4 films depend on the structure and the content in oxygen. As for the electrical resistivity (1.46×10^{-1} Ω.cm) found of the film, whose deposition time took 4 min, it is probably due to an increase in oxygen content and adsorbed close to the film surface. Furthermore, under ambient conditions, Co_3O_4 films adsorb oxygen from the air and create surface states. These surface states allow the electron to be excited from the valence band and, therefore, more holes are induced (in addition to holes induced by the non-stoichiometry of the oxygen lattice) in p-type Co_3O_4 crystallites. This result goes well with the EDS data (Fig. 6). Yadav et al. [38] studied the impact of substrate temperature for the film resistivity, and concluded that the microstructure of the films performs an interesting part on the electrical properties of a semiconductor

Table 2 Electrical resistivity, Hall mobility, carriers' concentration and thickness of the prepared Co_3O_4 thin films

Sample	Resistivity, (Ω.cm)	Hall mobility, (cm^2/Vs)	Carrier concentration, (cm^{-3})	Thickness, (nm)
4 min	1.46×10^{-1}	0.29	2.70×10^{17}	450
5 min	2.22	1.03	1.99×10^{16}	504
6 min	5.834	2.68	3.123×10^{15}	663
8 min	7.94	6.23	2.414×10^{14}	913

oxide. Moreover, Martínez-Gil et al. [39] have elaborated Co_3O_4 films by chemical solution deposition at different annealing temperatures of 200–400 °C. They reported that the resistivity of the films decreases (4.29×10^3 to 1.46×10^4 Ω.cm) ; possibly this is due to the incorporation of oxygen in the films that in turn generates holes that reduce the resistivity of the films. The possible factor that may contribute to the increase in resistivity is the reduction in dislocation density. This decrease can lead to a more ordered crystal structure. This observation is consistent with the Urbach energy data presented in Table 1. Although this can have a positive impact on charge carrier mobility (Table 2), the simultaneous reduction diffusion sites can also play a role in increasing resistivity. Furthermore, larger crystal grains, associated with an increase in crystallite size, can influence the interactions between charge carriers and grain boundaries. Additionally, diffraction of charge carriers through larger crystallites can also contribute to the increased resistivity. Moreover, the augmentation in resistivity can be attributive to an augmentation in Co^{+3} with increasing deposition times. This reduces the holes responsible for electrical conduction by hopping. It is essential to highlight a little article on the resistivity values of cobalt oxide thin films deposited by spray pyrolysis. However, research on cobalt oxide films deposited by sputtering [40] and atomic layer deposition [41] highlights high resistivity values, ranging between 100 and 10^2 (Ω.cm) compared to our study. This finding is explained by X-ray diffraction analyses, which reveal that current thin films, compared to other deposition methods, exhibit high crystalline with large crystals and a low amount of grain boundaries.

Figure 10 shows how the crystallite size and the mobility vary as function of the time taken to deposit the film. It is observed that mobility is augmented from 0.29 to 6.23 cm^2/Vs with the augmentation in the crystallite height which is attended by a diminution in corn confines. It is to remind that the electrical transport estates of films are ruled by carrier trappings at corn limits and belongs fundamentally on the morphology of the material and the status of evidence.

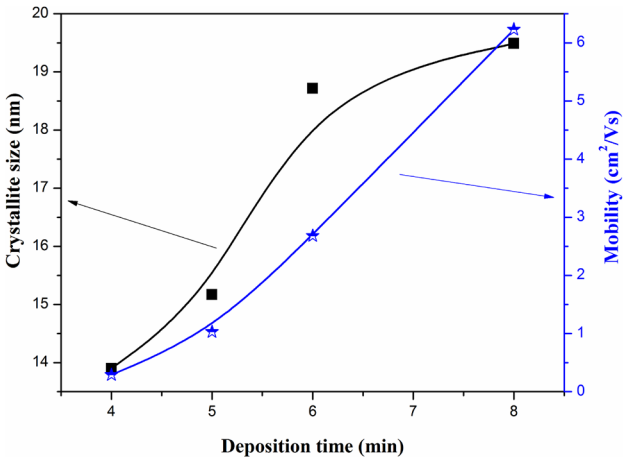

Fig. 10 Variations of crystallite size and mobility versus deposition lasting time

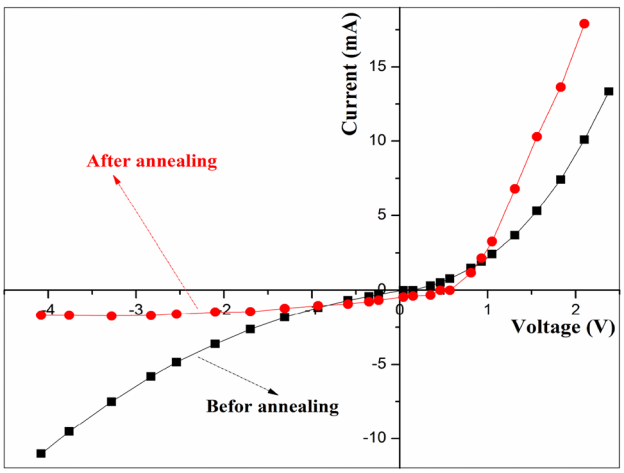

Fig. 11 I–V characteristics measured in darkness before and after annealing of the hetero-junction p-Co_3O_4/n-ZnO

3.4 I–V characteristics

3.4.1 Current–voltage under darkness

Figure 11 depicts the current–voltage representatives recorded for the structure p-Co_3O_4/n-ZnO prior and after annealing at 300 °C for 60 min. Herein, the film used in this structure is whose deposition time lasted 8 min. As shown in the Figure, the obtained curves advertise a rectifying diode behavior, an indication of a hetero-junction successful realization. Prior to annealing, the structure presented a high reverse current. This large leakage current is probably due to localized states at the p-Co_3O_4/n-ZnO interface. Following the annealing process, an improvement in the I–V characteristic is observed and is due probably to defects healing that led to the reduction of the interface states located at the level of the junction causing the leakage current.

The analysis of the apparatus current–voltage (I–V) representatives brings out useful data on the junction parameters like: series resistor (R_s), ideality factor

(n), saturation current (I_s). These are depicted by the relation:

$$I(V) = I_s\left(\exp\left(\frac{qV}{nkT}\right) - 1\right), \quad (3)$$

here k is the Boltzmann constant, T the absolute temperature, q the basic electronic charge, n the perfect coefficient and I_s the saturation current.

The perfect coefficient, n, has been obtained from the slope of the linear portion of the plot of front deformed diode event and is specified as:

$$n = \frac{q}{kT}\left(\frac{dV}{d(\ln(I))}\right) \quad (4)$$

According to the data presented in Table 3, the process of annealing led to a diminution in the series resistance and an augmentation in the saturation current. This is due to an improvement of the interface quality, either of structural origin or a readjustment of impurities. The increase in I_s with the temperature is due to the recombination of free carriers at the interface, that has also originated a decrease in the short circuit current (I_{sc}) [38]. The perfect coefficient (n) is determined according to Schottky diode equation and typically scales between 1 and 2, taking down on the manufacture process and semiconductor, it is utilized to establish which transport mechanism through the hetero-junction is prevailing. When n is equal to 1, diffusion is the main mechanism, however when $n < 2$, recombination and generation in the depletion layer is the prevailing. Based on the obtained ideality factor value of 1.64 (> 1) after annealing, this indicates that the generation-recombination process at the depletion layer is the dominant transport mechanism in the hetero-junction. However, before annealing the $n = 3.87$ (> 2), this proposes the attendance of interface states and defects in the interval of charge area that act as traps for charge transporters [42–44].

The realized devices were tested under illumination using a diodoscope (Tektronix), which is equipped with a halogen lamp of 100 mWcm^{-2} intensity. Figure 12 shows the current–voltage characteristic measurements at room temperature of the p-n heterojunction for the Co_3O_4 film deposited at 8 min with and without light. The photoelectric effect is clearly noticeable by looking at the I–V characteristics; the downward shift of the I–V characteristic is typical in solar cells' behavior under illumination. From Fig. 12, the open circuit voltage (V_{oc}) is equal to 369 mV and the short circuit current (I_{sc}) is being 1.302 mA. These values yield a fill factor FF of 32%. The same behavior was observed by Rana et al. [45] by studying Co_3O_4/ZnO hetero-junctions deposited by the sputtering deposition technique, under the light illumination. The p-Co_3O_4/n-ZnO shows a prominent photovoltaic effect with V_{oc} = 165 mV and I_{SC} = 76 µA. It's noteworthy that we observe an enhancement in the photovoltaic parameters achieved in this study under light excitation. This improvement serves as evidence of the efficacy of our absorbent material, which is derived from cobalt oxide produced through spray pyrolysis, in comparison to the supporting method.

Table 3 Electrical transport parameters of the heterojunction p-Co_3O_4/n-ZnO before and after annealing without light

Hetero-junction FTO/ZnO/Co_3O_4/Au	R_s, (Ω)	n	I_s, (A)
Before annealing	88.26	3.87	4.193×10^{-4}
After annealing	63.69	1.64	1.25×10^{-3}

4 Conclusions

In the present investigation, we have studied the impact of the deposition time on the structural, morphological, optical and electrical properties of thin layers of Co_3O_4 deposited on glass substrates utilizing the spray pyrolysis technique. X-ray diffraction

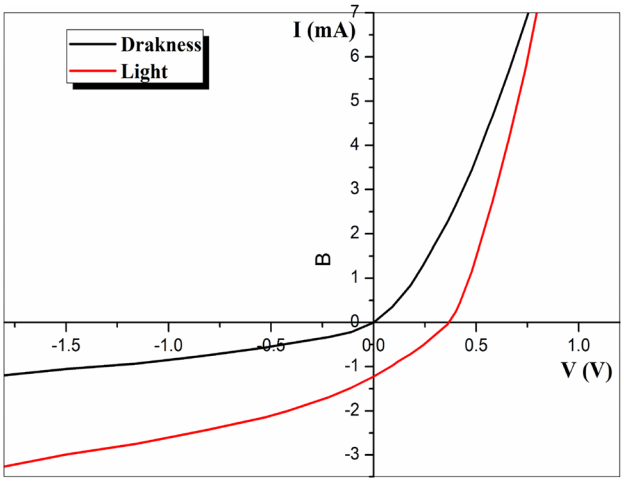

Fig. 12 I–V characteristics of the hetero-junction FTO/ZnO/Co_3O_4 with and without light

revealed polycrystalline kind for all films with a favored crystalline orientation along the (311) plane once the deposition time was varied between 4 and 8 min. The crystallite size is smaller with augmenting the deposition time. Raman spectroscopy confirmed Co_3O_4 films' single-phase structure. The morphological analysis carried out using SEM has clearly illustrated the high porosity character observed in the film deposited at 4 min. Meanwhile, the film, whose deposition time took 8 min, depicted a dense surface that contains irregular spindle grains, which were randomly distributed all over it. The transmittance of elaborated thin films diminished with longer time taken in the deposition. The band gap changed between 1.27 and 1.43 eV in the low-energy region, while in the high-energy region, the gap varied between 1.47 and 2.02 eV. The films, whose synthesis took 8 min, exhibited a gap energy value of 1.27 eV and a strong absorption at lower wavelengths, that is appropriate for solar cells applications. The films were all p-type conducting. Their conductivity and free carrier concentration decreased with augmenting the deposition time. A hetero-junction structure p-Co_3O_4/n-ZnO has been realized, based on the film whose deposition time was 8 min, and subjected to a heat treatment process. The hetero-junction exhibited a good rectifying conduct with a perfect coefficient varying between 3.87 and 1.64. The heat treatment has significantly improved the electrical properties of the hetero-junction by reducing its reverse current and its series resistance. The best optoelectric results are obtained for the cobalt oxide film produced at 8 min which allows the creation of the p-Co_3O4/n-ZnO junction where the photovoltaic characteristics are: V_{oc} = 369 mV in open circuit, I_{sc} = 1.302 mA and FF = 28%. A comparison with the results reported in the literature against the deposition method clearly indicates that the spray pyrolysis technique shows improvement in different characterizations.

Acknowledgements

The authors acknowledge the support from the Directorate-General for Scientific Research and Technological Development (DGRSDT-Algeria). This work has been carried out within the framework of PRFU projects N° A10N01UN280120220009 and N° A10N01UN190120220004 (MESRS-Algeria).

Author contributions

All authors contributed to the study conception and design. Material preparation, data collection and analysis were performed by WD, KM, NG, FZS and AZ. The first draft of the manuscript was written by WD, and all authors commented on previous versions of the manuscript. All authors read and approved the final manuscript.

Funding

This study was funded by the Directorate-General for Scientific Research and Technological Development (DGRSDT-Algeria) (PRFU projects N° A10N01UN280120220009 and N° A10N01UN190120220004) (MESRS-Algeria).

Data availability

The data that support the findings of this study are available from the corresponding author on reasonable request or as per journal policy.

Declarations

Conflict of interest The authors declare that they have no known competing financial interests or personal relationships that could have appeared to influence the work reported in this paper. The manuscript has not been published previously and is not under consideration for publication. It is also stated that the work is original. The publication is approved by all authors and tacitly or explicitly by the responsible authorities where the work was carried out. If accepted, it will not be published elsewhere in the same form, in English or in any other language, including electronically without the written consent of the copyright holder. In addition, the authors have no conflicts of interest nor data fabrication or reproducibility concerns and plagiarism.

References

1. B. Tatar, D. Demiroglu, K. Kazmanli, M. Ürgen, Improvement in electrical and photovoltaic properties of a-Si/c-Si

heterojunction with slanted nano-columnar amorphous silicon thin films for photovoltaic applications. Curr. Appl. Phys. **15**, 511–519 (2015). https://doi.org/10.1016/j.cap.2015.02.007
2. W. Daranfed, M.S. Aida, N. Attaf, J. Bougdira, H. Rinnert, Cu_2ZnSnS_4 thin films deposition by ultrasonic spray pyrolysis. J. Alloys Compd. **542**, 22–27 (2012). https://doi.org/10.1016/j.jallcom.2012.07.063
3. C.R. Kim, S.Y. Han, C.H. Chang, T.J. Lee, S.O. Ryu, Synthesis and characterization of $CuInSe_2$ thin films for photovoltaic cells by a solution-based deposition method. Curr. Appl. Phys. **10**, S383–S386 (2010). https://doi.org/10.1016/j.cap.2010.01.006
4. H. Alrashidi, A. Ghosh, W. Issa, N. Sellami, T.K. Mallick, S. Sundaram, Evaluation of solar factor using spectral analysis for CdTe photovoltaic glazing. Mater. Lett. **237**, 332–335 (2019). https://doi.org/10.1016/j.matlet.2018.11.128
5. W.W. Zhang, H. Qi, Y.K. Ji, M.J. He, Y.T. Ren, Y. Li, Boosting photoelectric performance of thin film GaAs solar cell based on multi-objective optimization for solar energy utilization. Sol. Energy. **230**, 1122–1132 (2021). https://doi.org/10.1016/j.solener.2021.11.031
6. M.S.H. Othman, E.B. Elkenany, Structural and optical properties of GaAs and InAs for doping sb under the effect of pressure and temperature: DFT and EPM investigations. Opt. Quant. Electron. **54**, 807 (2022). https://doi.org/10.1007/s11082-022-04203-8
7. N.N. Jandow, M.S. Othman, N.F. Habubi, S.S. Chiad, K.A. Mishjil, I.A. Al-Baidhany, Theoretical and experimental investigation of structural and optical properties of lithium doped cadmium oxide thin films. Mater. Res. Express. **6**, 116434 (2019). https://doi.org/10.1088/2053-1591/ab4af8
8. D. Ursu, M. Vajda, M. Miclau, Investigation of the p-type dye-sensitized solar cell based on full Cu_2O electrodes. J. Alloys Compd. **802**, 86–92 (2019). https://doi.org/10.1016/j.jallcom.2019.06.180
9. T. Miyata, H. Tokunaga, K. Watanabe, N. Ikenaga, T. Minami, Photovoltaic properties of low-damage magnetron-sputtered n-type ZnO thin film/p-type Cu_2O sheet heterojunction solar cells. Thin Solid Films. **697**, 137825 (2020). https://doi.org/10.1016/j.tsf.2020.137825
10. W. Daranfed, N. Guermat, K. Mirouh, Experimental study in the effect of precursors in Co_3O_4 thin films used as solar absorbers. Ann. Chim. -Sci Mat. **44**, 121–126 (2020). https://doi.org/10.18280/acsm.440207
11. A. Lakehal, B. Benrabah, A. Bouaza, C. Dalache, B. Hadj, Tuning of the physical properties by various transition metal doping in Co_3O_4: TM (TM = ni, Mn, Cu) thin films: a comparative study. Chin. J. Phys. **56**, 1845–1852 (2018). https://doi.org/10.1016/j.cjph.2018.08.012
12. X.T. Zhang, X.Z. Chen, G. Luo, L. Li, Y. Li, J.N. Hu, B.J. Zhang, Co_3O_4-based fluffy tubes structure used as anode material for lithium-ion Battery. Mater. Lett. **309**, 131427 (2022). https://doi.org/10.1016/j.matlet.2021.131427
13. E. Turan, E. Zeybekoglu, M. Kul, Effects of bath temperature and deposition time on Co thin films produced by chemical bath deposition. Thin Solid Films **692**, 137632 (2019). https://doi.org/10.1016/j.tsf.2019.137632
14. V.S. Devi, M. Athika, E. Duraisamy, A. Prasath, A.S. Sharma, P. Elumalai, Facile sol-gel derived nanostructured spinel Co_3O_4 as electrode material for high-performance supercapattery and lithium-ion storage. J. Energy Storage. **25**, 100815 (2019). https://doi.org/10.1016/j.est.2019.100815
15. A. Louardi, A. Rmili, F. Ouachtari, A. Bouaoud, B. Elidrissi, H. Erguig, Characterization of cobalt oxide thin films prepared by a facile spray pyrolysis technique using perfume atomizer. J. Alloys Compd. **509**, 9183–9189 (2011). https://doi.org/10.1016/j.jallcom.2011.06.106
16. R. Balakarthikeyan, A. Santhanam, K. Vibha, M. Shkir, H. Algarni, I.M. Ashraf, M. Kumar, M.R.V. Reddy, Noticeable effect of coating temperature on Co_3O_4 thin films developed through low-cost nebulizer spray pyrolysis for photo-sensing applications. Surf. Inter. **38**, 102849 (2023). https://doi.org/10.1016/j.surfin.2023.102849
17. M. Manickam, V. Ponnuswamy, C. Sankar, R. Suresh, R. Mariappan, J. Chandrasekaran, The effect of solution pH on the properties of cobalt oxide thin films prepared by nebulizer spray pyrolysis technique. Int. J. Thin Fil Sci. Tec. **5**(3), 155–161 (2016). https://doi.org/10.18576/ijtfst/050302
18. M. Patel, J. Kim, Thickness-dependent photoelectrochemical properties of a semitransparent Co_3O_4 photocathode. Beilstein J. Nanotechnol. **9**, 2432–2442 (2018). https://doi.org/10.3762/bjnano.9.228
19. R. Manogowri, R. Mary Mathelane, S. Valanarasu, I. Kulandaisamy, A. Benazir Fathima, A. Kathalingam, Effect of annealing temperature on the structural, morphological, optical and electrical properties of Co_3O_4 thin film by nebulizer spray pyrolysis technique. J. Mater. Sci. : Mater. Electron. **27**, 3860–3866 (2016). https://doi.org/10.1007/s10854-015-4234-2
20. N. Guermat, W. Daranfed, I. Bouchama, N. Bouarissa, Investigation of structural, morphological, optical and electrical properties of Co/Ni co-doped ZnO thin films. J. Mol. Struct. **1225**, 129134 (2021). https://doi.org/10.1016/j.molstruc.2020.129134

21. W. Darenfad, N. Guermat, K. Mirouh, Thoughtful investigation of ZnO doped mg and co-doped Mg/Mn, Mg/Mn/F thin films: a first study. J. Mol. Struct. **1286**, 135574 (2023). https://doi.org/10.1016/j.molstruc.2023.135574
22. M.S. Othman, K.A. Mishjil, H.G. Rashid, S.S. Chiad, N.F. Habubi, I.A. Al–Baidhany, Comparison of the structure, electronic, and optical behaviors of tin–doped CdO alloys and thin films. J. Mater. Sci. : Mater. Electron. **31**, 9037–9043 (2020). https://doi.org/10.1007/s10854-020-03437-0
23. T. Prasada Rao, M.C. Santhoshkumar, Effect of thickness on structural, optical and electrical properties of nanostructured ZnO thin films by spray pyrolysis. Appl. Surf. Sci. **255**, 4579–4584 (2009). https://doi.org/10.1016/j.apsusc.2008.11.079
24. W. Darenfad, N. Guermat, K. Mirouh, A comparative study on the optoelectronic performance of undoped, Mg-doped and F/Mg co-doped ZnO nanocrystalline thin films for solar cell applications. J. Nano Electron. Phys. **13**, 06016 (2021). https://doi.org/10.21272/jnep.13(6).06016
25. M. Khalfallah, N. Guermat, W. Daranfed, N. Bouarissa, H. Bakhti, Hydrophilic nickel doped porous SnO_2 thin films prepared by spray pyrolysis. Phys. Scr. **95**, 095805 (2020). https://doi.org/10.1088/1402-4896/aba8c5
26. C. Ravi Dhas, R. Venkatesh, R. Sivakumar, A. Moses Ezhil Raj, C. Sanjeeviraja, Effect of solution molarity on optical dispersion energy parameters and electrochromic performance of Co_3O_4 films. Opt. Mater. **72**, 717–729 (2017). https://doi.org/10.1016/j.optmat.2017.07.026
27. M. Boucharda, A. Gambardellab, Raman microscopy study of synthetic cobalt blue spinels used in the field of art. J. Raman Spectrosc. **41**, 1477–1485 (2010). https://doi.org/10.1002/jrs.2645
28. T.A. Mulinari, F.A.L. Porta, J. Andr, M. Cilense, J.A. Varela, E. Longo, Microwave hydrothermal synthesis of single-crystalline Co_3O_4 spinel nanocubes. Cryst. Eng. Comm. **15**, 7443–7449 (2013). https://doi.org/10.1039/C3CE41215F
29. P.J. Murray, J.W. Linnett, Mössbauer studies in the spinel system $co_xfe_{3-x}o_4$. J. Phys. Chem. Solids. **37**, 619–624 (1976). https://doi.org/10.1016/0022-3697(76)90111-6
30. I.H. Jung, S.A. Decterov, A.D. Pelton, H.M. Kim, Y.B. Kang, Thermodynamic evaluation and modeling of the Fe–Co–O system. Acta Mater. **52**, 507–519 (2004). https://doi.org/10.1016/j.actamat.2003.09.034
31. V.G. Hadjiev, M.N. Iliev, I.V. Vergilov, The Raman spectra of Co_3O_4. J. Phys. **21**, L199 (1988). https://doi.org/10.1088/0022-3719/21/7/007
32. N.E. Rajeevan, R. Kumar, D.K. Shukla, R.J. Choudhary, P. Thakur, A.K. Singh, S. Patnaik, S.K. Arora, I.V. Shvets, P.P. Pradyumnan, Magnetoelectric behavior of ferrimagnetic $Bi_xCo_{2-x}MnO_4$ (x = 0, 0.1 and 0.3) thin films. J. Magn. Magn. Mater. **323**, 1760–1765 (2011). https://doi.org/10.1016/j.jmmm.2011.01.032
33. N. Kouidri, S. Rahmane, A. Allag, Substrate temperature-dependent properties of sprayed cobalt oxide thin films. J. Mater. Sci: Mater. Electron. **30**, 1153–1160 (2019). https://doi.org/10.1007/s10854-018-0384-3
34. A. Lakehal, B. Bedhiaf, A. Bouaza, H. Benhebal, A. Ammaric, C. Dalache, Structural, optical and electrical properties of Ni-doped Co_3O_4 prepared via Sol-Gel technique. Mat. Res. **21**, 20170545 (2018). https://doi.org/10.1590/1980-5373-MR-2017-0545
35. O. Gencyılmaz, T. Taskopru, F. Atay, I. Akyuz, Synthesis, characterization and ellipsometric study of ultrasonically sprayed Co_3O_4 films. Appl. Phys. A **121**, 245–254 (2015). https://doi.org/10.1007/s00339-015-9417-4
36. V. Patil, P. Joshi, M. Chougule, S. Sen, Synthesis and characterization of Co_3O_4 thin Film, Soft. Nanosci. Lett. **2**, 1–7 (2012). https://doi.org/10.4236/snl.2012.21001
37. V.R. Shinde, S.B. Mahadik, T.P. Gujar, C.D. Lokhande, Supercapacitive cobalt oxide (Co_3O_4) thin films by spray pyrolysis. Appl. Surf. Sci. **252**, 7487–7492 (2006). https://doi.org/10.1016/j.apsusc.2005.09.004
38. A.A. Yadav, U.J. Chavan, Electrochemical supercapacitive performance of spray deposited Co_3O_4 thin film nanostructures. Electrochim. Acta. **232**, 370–376 (2017). https://doi.org/10.1016/j.electacta.2017.02.157
39. M. Martínez-Gil, D. Cabrera-German, M.I. Pintor-Monroy, J.A. García-Valenzuela, M. Cota-Leal, W. De la Cruz, M.A. Quevedo-Lopez, R. Perez-Salas, M. Sotelo-Lerma, Effect of annealing temperature on the thermal transformation to cobalt oxide of thin films obtained via chemical solution deposition. Mater. Sci. Semicond. Process. **107**, 104825 (2020). https://doi.org/10.1016/j.mssp.2019.104825
40. H.E. Aakib, J.F. Pierson, M. Chaik, C. Samba Vall, H. Ait Dads, A. Narjis, A. Outzourhit, Evolution of the structural, morphological, optical and electrical properties of reactively RF-sputtered cobalt oxide thin films with oxygen pressure. Vacuum. **159**, 346–352 (2019). https://doi.org/10.1016/j.vacuum.2018.10.065
41. K.B. Klepper, O. Nilsen, H. Fjellvag, Growth of thin films of Co_3O_4 by atomic layer deposition. Thin Solid Films. **515**, 7772–7781 (2007). https://doi.org/10.1016/j.tsf.2007.03.182
42. S. Mali, P.S. Shinde, C.A. Betty, P.N. Bhosale, Y.W. Oh, P.S. Patil, Synthesis and characterization of Cu_2ZnSnS_4 thin films by SILAR method. J. Phys. Chem. Solids. **73**, 735–740 (2012). https://doi.org/10.1016/j.jpcs.2012.01.008
43. M. Brotzmann, U. Vetter, H.J. Hofsass, BN/ZnO heterojunction diodes with apparently giant ideality factors. Appl.

Phys. **106**, 063704 (2009). https://doi.org/10.1063/1.3212987

44. A. Schenk, H.J. Krumbein, Coupled defect-level recombination: theory and application to anomalous diode characteristics. Appl. Phys. **78**, 3185 (1995). https://doi.org/10.1063/1.360007
45. A.K. Rana, M. Patel, T.T. Nguyen, J.H. Yun, J. Kim, Transparent Co_3O_4/ZnO photovoltaic broadband photodetector. Mater. Sci. Semicond. Process. **117**, 105192 (2020). https://doi.org/10.1016/j.mssp.2020.105192